Shock wave study of the $\alpha \rightleftarrows \varepsilon$ phase transition in iron

L. M. Barker, and R. E. Hollenbach

Citation: Journal of Applied Physics **45**, 4872 (1974); doi: 10.1063/1.1663148
View online: https://doi.org/10.1063/1.1663148
View Table of Contents: http://aip.scitation.org/toc/jap/45/11
Published by the American Institute of Physics

Shock wave study of the $\alpha \rightleftarrows \epsilon$ phase transition in iron*

L. M. Barker† and R. E. Hollenbach

Sandia Laboratories, Albuquerque, New Mexico 87115
(Received 17 June 1974)

Plate impact experiments producing plane waves of up to 40 GPa (400 kbar) peak stress were performed using Armco iron specimens and impactors. Highly accurate time-resolved measurements of the resulting free-surface velocities of the specimens were obtained with the VISAR laser interferometer instrumentation system. The free-surface velocity profiles provide new information concerning the rate effects associated with the $\alpha \rightarrow \epsilon$ polymorphic phase transition at 13 GPa, the material strength and release wave speeds at 10 and 40 GPa, and the stress level at which the iron reverts back to the α phase on unloading. A strong magnetic field was found to produce no measurable change in the phase-transition stress. The accuracy of the "factor-of-2" assumption relating free-surface velocity to particle velocity in iron was also evaluated experimentally.

I. INTRODUCTION

Bancroft, Peterson, and Minshall[1] reported stable three-wave shock structures in iron shocked to about 20 GPa (200 kbar). They interpreted their results as indicating a polymorphic phase transition in iron at about 13 GPa when shocked from room temperature and pressure. Subsequent static high-pressure experiments using x-ray diffraction[2-4] determined that at room temperature iron transforms under pressure from the initial bcc, or α phase, to the hcp, or ϵ phase. Other shock wave studies of iron completed its Hugoniot curve from 0 to 1000 GPa,[5-13] but the only additional detailed picture of the shock wave structure which evolves as a result of the phase transition came from a single free-surface velocity profile published by Novikov *et al.*[14]

The existing experimental data on rate effects in the phase change have been quite puzzling, as was pointed out by Horie and Duvall,[15] for whereas Clendenen and Dirckamer[4] reported the $\alpha \rightarrow \epsilon$ transition to be "sluggish" under quasistatic pressures, the transition obviously occurs in the submicrosecond time scale in shock experiments. It has been presumed that the large and rapid shear deformation experienced in shock wave experiments can strongly affect the phase-transition rate. However, Horie and Duvall[16] also noted that even among the shock wave studies the apparent characteristic time of the phase transition varies from about 0.01 μsec to tens of μsec. They suggested that more precise experimental data on shock amplitudes and wave profiles in iron would help clarify the issue.

As a result of recent advances in laser interferometer instrumentation,[17] it has become possible to obtain detailed measurements of the time-resolved velocity of the free surfaces of shock-loaded specimens. Laser interferometry, therefore, has been used in a new shock wave study of the polymorphic phase transition in iron. The principal objectives of the study were to provide some answers to the phase-transition rate questions and to learn more about yield strengths and release wave speeds at stresses above 10 GPa. Another objective was to provide an independent check of the results of Curran,[18] who reported a marked decrease in the $\alpha \rightarrow \epsilon$ phase-transition stress as a result of a strong magnetic field applied to the iron specimen during shock loading.

Although the analysis of the experimental data in this paper is by no means exhaustive, most of the objectives of the study have been attained. In addition, there was an unexpected bonus: it was possible to use the detailed free-surface velocity profiles to deduce a reasonably accurate value for the stress at which the high-pressure ϵ phase begins transforming back into the α phase upon unloading. This is the first shock wave determination of the reverse transformation stress in iron, and it appears to provide a more accurate measure than previous quasistatic high-pressure experiments by Giles *et al.*[19] and by Takahashi *et al.*[20]

In Sec. II of this paper we review the experimental details of the study, and Sec. III presents the measured data. Some analyses and discussions of various aspects of the data are given in Sec. IV, including the stress level at the onset of the $\alpha \rightarrow \epsilon$ phase change, the validity of the "factor-of-2" relation between free-surface velocity and internal particle velocity, the $\alpha \rightarrow \epsilon$ phase change relaxation time, sound speed and yield strength findings, Hugoniot and release path determinations including the stress at the onset of the $\epsilon \rightarrow \alpha$ reverse phase change, and the effect of a nearly saturating magnetic field on the $\alpha \rightarrow \epsilon$ phase transition. Some concluding remarks are presented in Sec. V.

II. EXPERIMENTAL

The Armco iron used in these experiments had a purity of 99.8%, an average grain size of 150 μm, and a density of 7.85 g/cm^3. All of the sample plates were cut from the center 35 mm of a 41-mm-thick flat stock. The plates were cut parallel to the plane of the stock. The material was used as-recieved, that is, without additional heat treating or annealing. The sample hardness was Rockwell B 34 to 37.

The data were collected from experiments conducted with one of Sandia Laboratories' high-velocity powder gun facilities. The gun has a barrel length of 17.8 m and a bore diameter of 89 mm. Controlled impacts in the velocity range 0.4–2.5 mm/μsec are available with this bore diameter, and much higher velocities can be attained when the gun is used in a two-stage mode with smaller bore barrels.

The experimental configuration just before impact is illustrated in Fig. 1. The impact velocities are measured to about $\pm 0.2\%$ by the successive shorting of charged electrical probes by the metal projectile nose plate. The gun barrel and impact chamber are evacuated

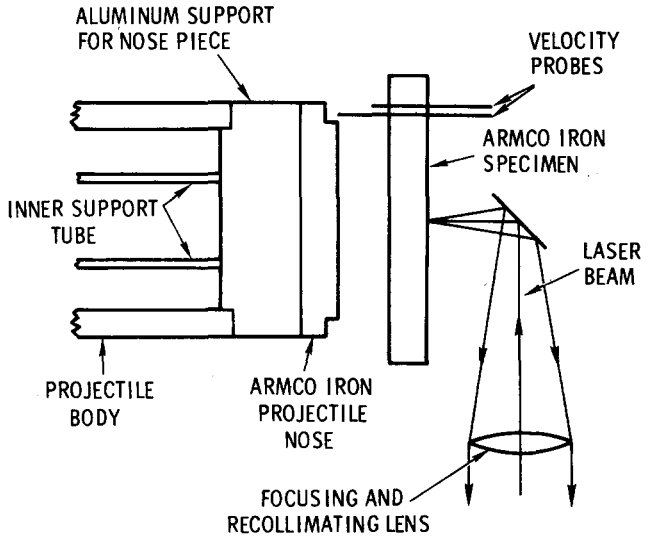

FIG. 1. Schematic of the experimental configuration just prior to impact. The velocity probes contacted the projectile nose in the outside recessed ring to prevent any ejection of material into the central impact region. The aluminum support for the nose piece was omitted when the nose piece was at least 12 mm thick. The diameter of the impact area of the projectile nose was always 77.8 mm. This diameter should be used in computing the arrival time of edge effects at the measuring station.

before each shot to a pressure of 13 Pa (100 μm Hg) or less to minimize any slow pressure buildup just before impact. The impact surface of the projectile and both surfaces of the specimen were lapped flat to better than 2.5 μm over a diameter of 75 mm. An adjustable specimen mounting fixture makes it possible to align the impact surface of the specimen parallel to the nose of the projectile while the projectile is in the barrel. As a result, the tilt between the impacting surfaces averages less than 1.5 mrad.

The profiles of the transmitted waves were obtained in the form of surface velocity vs time using the Velocity Interferometer System for Any Reflector (VISAR).[17,21,22] The VISAR measures the velocity history of a very small area on the specimen surface by recording the light fringes produced in its interferometer. The fringes result from the Doppler shift imparted to the wavelength of a focused laser beam by the motion of the specimen surface. In this interferometer, the number of fringes is proportional to the surface velocity, and the fringe frequency is proportional to the surface acceleration. The equation relating the velocity to the fringe count for free-surface experiments is[22]

$$v(t-\tfrac{1}{2}t_d)=\frac{\lambda F(t)}{2t_d(1+\delta)}, \tag{1}$$

where λ is the original wavelength of the laser light, $F(t)$ is the number of fringes produced up to time t, t_d is the time by which the light traversing one of the legs of the interferometer is delayed with respect to the light traversing the other interferometer leg, and the factor $(1+\delta)$ corrects for the index-of-refraction dispersion effect in the etalon in the delay leg of the interferometer.[22] The delay times t_d for the experiments of this study were always about 2 nsec or less. The almost negligible-$\frac{1}{2}t_d$ correction of the time of the velocity in Eq. (1) properly centers the velocity timing relative to that of the fringe count, $F(t)$.[23]

A key feature of the VISAR is that it can monitor the velocity of either spectrally reflecting or diffusely reflecting specimen surfaces, as its name implies. Earlier laser interferometer instrumentation techniques[23–25] were limited to those cases in which a mirror finish could be maintained on the specimen during the experiment. Such techniques had failed when tried on iron because the arrival of the phase-transition wave adversely affected the mirror finish on the specimen. With the VISAR, however, an initially diffuse specimen surface could be used and its reflectivity remained nearly constant during the experiment.

In two of the experiments for this study, a sapphire "window" was cemented to the VISAR-monitored specimen surface in order to prevent most of the reflection of the incident stress wave by eliminating the free surface. For these experiments, an additional factor of $(1+\Delta\nu/\nu_0)$ should appear in the denominator of Eq. (1) to correct for the stress-wave-induced change in the index of refraction of the sapphire window.[23] These two experiments are discussed in greater detail in Sec. III of this paper.

The VISAR measured the surface velocities with a precision of ± 0.003 mm/μsec or better. The rise time of the instrumentation was about 7 nsec except for several recordings of the first plastic wave (P1) arrival where special high-frequency oscilloscopes and photomultipliers were used to achieve a rise time of about 2 nsec.

The preparation for the VISAR instrumented experiments was greatly aided by the use of a special purpose Synchronized Manual And Repetitive Test (SMART) box.[26] This unit causes the dual beam oscilloscopes to alternately display the photomultiplier data and the base lines of each channel at a 20-Hz repetition rate. As a result, the proper oscilloscope settings are much easier to achieve, and they can be checked and adjusted until just seconds before the firing of the gun. Actuating a single switch on the SMART box puts the oscilloscopes in the "ready" state for the shot. Immediately after the shot is fired, the SMART box automatically switches out the data signals, switches in time marks, resets the scopes, and retriggers the scopes to put time marks and base lines on the oscillograms. The SMART box not only simplifies the preparation of an experiment, but also increases the accuracy of the data by greatly decreasing the time during which the oscilloscopes can drift away from their correct settings.

The precision measurements of free-surface velocity by the VISAR are of limited value unless the time base on which the velocity is plotted can be accurately related to the time of impact. Two different methods were used for establishing the impact time. One method consisted of explicit measurements of the stress-wave transit time by means of very accurate time interval determinations. The impact time at the center of the flat specimen surface was assumed to be the average of the closure times of four electrical probes (not shown in Fig. 1) mounted flush with the specimen impact surface around the periphery of the impact area.[27] The closure of one of these probes was also used to generate a fidu-

TABLE I. Summary of experiments. Thicknesses are in mm. Velocities in mm/μsec, accelerations in mm/μsec², stress in GPa.

Experiment No.	Impactor thickness	Specimen thickness	Impact velocity	Peak stress	$\frac{V}{V_{0\min}}$	$\frac{u_{fm}}{u_m}$ [a]	u_{fs} [a] atop P1 wave	Stress atop P1 wave	Peak accel. in P1 wave [b]	Peak accel. in P2 wave [c]	P2 Lagrangian wave velocity
1	6.330	6.317	0.9916	17.3	0.8819	1.982	0.645	13.15	...	1.52	3.12
2	6.350	6.312	1.150	20.4	0.8697	1.976	0.652	13.30	...	4.00	3.72
3	19.14	15.82	0.997	17.3	0.8811	1.971	0.635	12.92	...	0.85	3.15
4	19.14	15.82	1.247	22.6	0.8633	1.968	0.637	12.96	...	4.66	4.08
5	6.314	6.314	1.292	23.6	0.8598	1.972	0.653	13.32	...	7.86	4.16
6	6.337	6.370	1.567	30.4	0.8411	1.978	0.667	13.60	...	26.1	4.76
7	12.82	19.14	1.292	23.7	0.8602	1.964	0.634	12.90	...	5.29	4.21
8	12.81	19.13	1.557	30.1	0.8418	1.967	0.640	13.02	...	14.8	4.77
9	6.337	6.345	1.900	39.6	0.8208	1.976	...	...	...	...	5.29
10	6.325	6.332	1.871	38.6	0.8220	1.971	...	...	...	...	5.24
11	6.330	19.07	1.887 [d]	39.1	0.8212	...	...	...	...	...	5.26
12	6.327	19.06	1.908	39.8	0.8203	1.969	...	...	...	...	5.29
13	6.320	6.380	0.6711	13.2	0.9316	1.988	0.640	13.05	39.2	...	...
14	6.335	6.375	0.6127	12.1	0.9396	1.987	...	...	...	...	...
15 [e]	3.185 [f]	6.304	0.4825	10.26	0.9482	...	...	...	14.2 [g]	...	...
16 [e]	3.170 [f]	6.309	0.6210	13.15	0.9365	...	...	...	37.8	...	...
17 [h]	6.426	6.380 [h]	1.307	24.0	0.8588	1.970	0.659	13.44	49.9	10.3	4.21
18 [e]	6.434	6.358 [h]	1.253	22.8	0.8630	1.972	0.653	13.32	49.4	7.90	4.08
19	19.15	15.76	1.396	26.1	0.8528	1.961	0.638	12.98	28.4	9.9	4.45
20	3.36 [i]	3.11	0.615	15.7	0.8935	...	0.673	13.74	...	0.67	2.41

[a] u_{fm} = peak free-surface velocity; u_m = peak particle velocity at impact plane; u_{fs} = free-surface velocity.
[b] As measured on the free surface using 2-nsec rise-time instrumentation.
[c] As measured on the free surface.
[d] Determined indirectly as mentioned in the text.
[e] These experiments used sapphire windows on the rear surface of the specimen.
[f] Sapphire impactor.
[g] Free-surface equivalent; the measured acceleration at the sapphire window was approximately half of this value.
[h] Specimen magnetized to near saturation.
[i] Tungsten carbide impactor.

cial light pulse[28] near the photocathodes of each of the VISAR photomultiplier tubes. By this method, the free-surface celocity records were related to the impact time to an accuracy of ±7 nsec. Two of the experiments on 15.8-mm-thick specimens used this timing method, and both also were in the impact velocity range for which both plastic (P1) and phase-transition (P2) waves were present. Both experiments gave a Lagrangian wave speed of 5.07 ± 0.01 mm/μsec for the midpoint of the P1 wave. This velocity is also in excellent agreement with other measurements of the 13-GPa P1 wave speed.[1,13,29]

The second method for establishing impact time makes use of prior knowledge of the propagation velocity of some part of the wave profile. Thus, having established that the 13-GPa P1 wave travels at 5.07 mm/μsec, and knowing the specimen thickness, one can find the time of impact relative to the time of arrival of the midpoint of the P1 wave. In this way, the plastic wave was used as a timing fiducial in a number of the experiments. The elastic wave could have been used instead, but the longer rise time of the elastic wave, its much smaller amplitude, and its greater variability in profile made it less satisfactory as a timing fiducial. Nevertheless, the elastic wave was used as the fiducial in four of the experiments which contained no 13-GPa P1 wave. In those cases, the timing was shifted until the profile of the initial rise of the elastic wave coincided as well as possible with the elastic waves of similar thickness specimens for which the timing had already been established as discussed above. The time intervals established in this way are estimated to be accurate to ± 0.5% or better.

III. MEASURED DATA

The velocity profile data obtained in this study are considerably more accurate in the region above 10 GPa than any which have appeared previously in the literature. Also, the data are reasonably comprehensive, having been obtained for differing specimen thicknesses and a reasonably uniform spectrum of peak stresses from 10 to 40 GPa. The analyses of these data in Sec. IV are for the most part of a preliminary nature, since very little fitting of the velocity profiles has been done by computer solutions of the wave propagation problems. Therefore, we shall present the experimental data in some detail in hopes that they may prove valuable to others who may wish to perform further analyses of their own. All of the measured wave profile figures below are reproduced directly from computer plots of the data to preserve, to the greatest extent possible, the

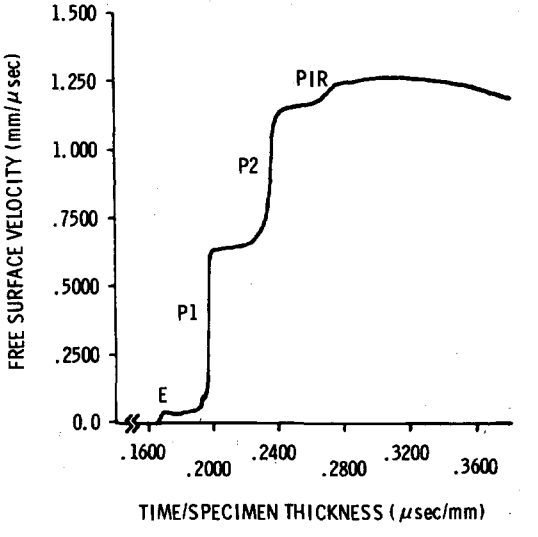

FIG. 2. Free-surface velocity history of experiment 7.

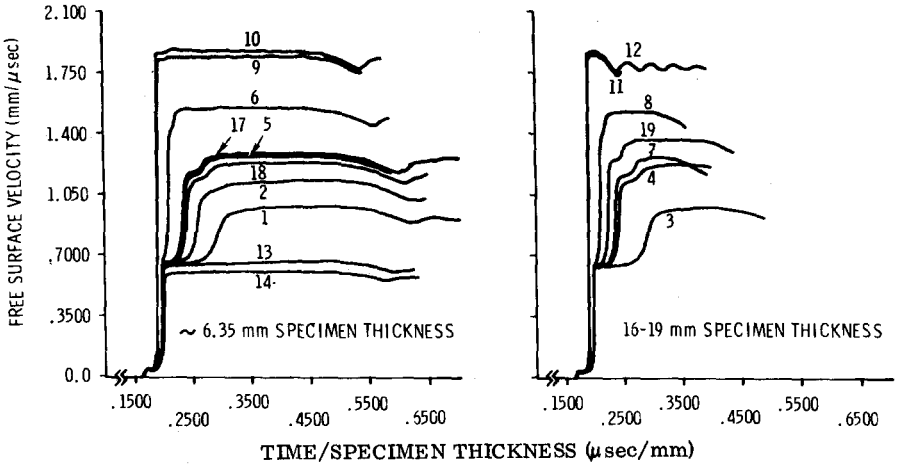

FIG. 3. Complete velocity profiles of all free-surface experiments except 20. The experiment number of each profile is indicated.

high resolution of the VISAR measurements.

Pertinent information about each of the experiments is given in Table I. The impact velocity measurement failed in experiment 11, but the free-surface velocity was accurately measured by the VISAR. Experiments 9, 10, and 12 all had approximately the same peak stress as experiment 11, and they provided good measurements of the ratio u_{fm}/u_m, where u_{fm} is the peak free-surface velocity and u_m is the peak particle velocity at the impact plane. Thus, knowing the value of u_{fm}/u_m from experiments 9, 10, and 12, and having measured u_{fm} on experiment 11, the value of u_m was calculated and was used in the determination of the peak stress and the corresponding volume. The value of u_m calculated in this way for experiment 11 is probably accurate to $\pm 0.3\%$, which is almost as good as the direct measurement would have been.

The free-surface velocity profiles were in general characterized by four major distinct velocity increases, as exemplified by the profile in Fig. 2. The first velocity increase, E, is caused by the arrival of the elastic precursor, or E wave. It produces a free-surface velocity of about 0.04 mm/μsec. The second major velocity increase, P1, results from the arrival of the first plastic wave, or P1 wave. The amplitude of this wave is indicative of the stress at the onset of the transition from the α to the ϵ phase. The third velocity increase, P2, is caused by the arrival of the phase transition wave, i.e., the wave which carries the material from the α phase to the peak stress level in the ϵ phase. Finally, a relatively small additional free-surface velocity increase, PIR, arrives as a result of a phase interface reflection. The experiments of this study are the first to resolve this important characteristic of the free-surface velocity profile. The PIR wave is an artifact of the free surface, and it would not be present if the time-resolved stress or particle velocity were measured *in situ*. The origin of the PIR wave is discussed in Sec. IV D.

Figure 3 shows superimposed plots of all of the VISAR-measured free-surface velocity profiles except for experiment 20.[30] The time axis in these plots and others to follow was normalized by dividing the actual time from impact by the specimen thickness.

Experiments 13 and 14 (Fig. 3) were at too low an impact velocity to produce an appreciable phase transition. In experiments 9—12 the impact velocity produced a stress of almost 40 GPa. At this stress, the velocity of the P2 wave is greater than that of the P1 wave, so no separate P1 wave ever forms. The rest of the free-surface experiments all show the P2 and PIR waves, although the PIR wave was very small and poorly defined in experiments 1 and 3. It can be seen that the velocity of the P2 wave increases with increasing peak particle velocity, and that the time between the P1 and P2 arrivals is always approximately equal to the time between the P2 and PIR arrivals.

Figure 4 shows magnified views of the elastic precur-

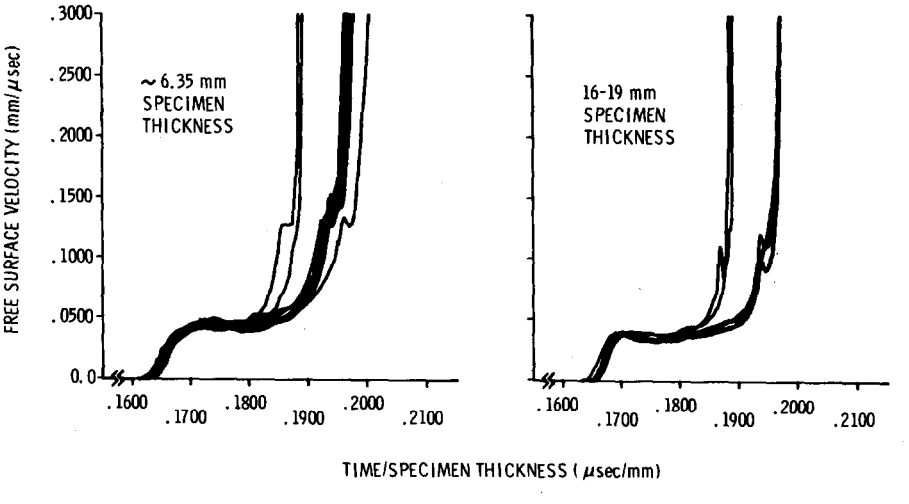

FIG. 4. Enlargements of the elastic precursor portions of Fig. 3.

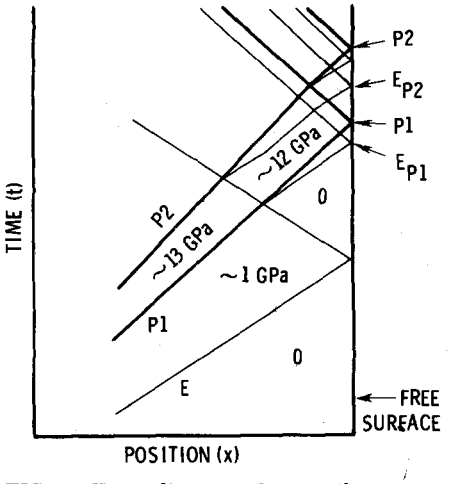

FIG. 5. Wave diagram showing the expected elastic wave arrivals at the free surface. The E_{P_1} wave is born at the interaction of the reflected E wave with the on-coming P1 wave. The E_{P2} wave is one of the expected elastic precursors of the P2 wave.

sor portions of Fig. 3. In each experiment except 20 a decrease in free-surface velocity was observed following an initial peak at about 0.04 mm/μsec. This was caused by the well-known stress overshoot of the elastic wave in iron.[12,31-33]

The relatively small perturbations in the profiles at free-surface velocities of 0.1 to 0.15 mm/μsec are caused by the arrival of a second elastic precursor of the P1 wave.[12] This precursor, which we shall call the E_{P_1} wave, originates at the interaction point of the reflected E wave with the oncoming P1 wave, as shown in the x,t diagram of Fig. 5. The reflected E wave leaves the iron next to the free surface essentially in its original zero stress and strain condition. Thus, after the interaction, the initial loading of the P1 wave is elastic, and a new elastic precursor is born. Two similar precursors of the P2 wave are also shown in Fig. 5.

The elastic wave profiles vary from one experiment to the next, particularly in the amplitude and shape of the E_{P_1} wave. This is probably due in part to the VISAR's measurement of the velocity of an area which is only about the size of one grain on the specimen surface (150 μm), rather than averaging the surface velocity over a large number of grains. Elastic wave perturbations on grain-size areas have also been detected by McQueen *et al.*,[34] using a streak camera technique.

An enlargement of the plateau region between the P1 and P2 waves of Fig. 3 is provided in Fig. 6. It is seen that for a given specimen thickness, the free-surface velocity in the plateau region increases with increasing peak stress level. The small oscillations in the profiles of experiments 2, 13, and 14 are artifacts of the data reduction procedure and represent small uncertainties in the velocity rather than actual velocity oscillations.

Figure 7 shows the area of Fig. 3 containing the top of the P1 wave, and the P2 and PIR waves. This figure is useful for determining the amplitudes of the P2 and PIR waves. Based on an x,t wave diagram (Fig. 5), one would expect to see two secondary elastic waves reaching the free surface between the P1 and P2 wave arrivals. What appears to be the E_{P_2} wave of Fig. 5 can be distinguished in some of the profiles, as pointed out in Fig. 7.

Experiments 15 and 16 of this study were designed to measure a particle velocity history which approximates that at a point internal to the sample where no free-surface effects are present. In these experiments, a clear sapphire "window" was cemented with a very thin layer of epoxy (no more than 2 μm thick) to the specimen surface, and the VISAR's laser beam was reflected from the iron-sapphire interface. Since the shock impedance of sapphire is very similar to that of iron, the wave reflections from the iron-sapphire interface were small. Therefore, the measured motion was not very different from the particle velocity history which would have been present inside the iron with no influence from interfaces or free surfaces.

The sapphire window was z cut and was elastic in the range of stresses encountered in these experiments. The stress-wave propagation properties of the sapphire within its elastic range are accurately known,[17] and thus it was relatively easy to correct the measured velocity profile to the internal particle velocity history of the iron. The resulting internal particle velocity profiles are shown in Fig. 8.

As indicated in Table I, the impactors in experiments 15 and 16 were also of sapphire. Therefore, since the

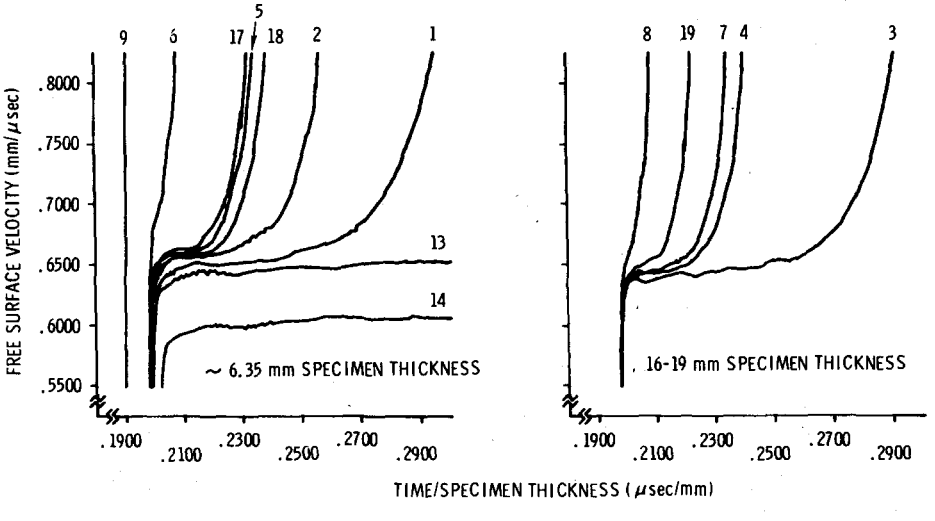

FIG. 6. Enlargements of the plateau region between the P1 and P2 waves in Fig. 3.

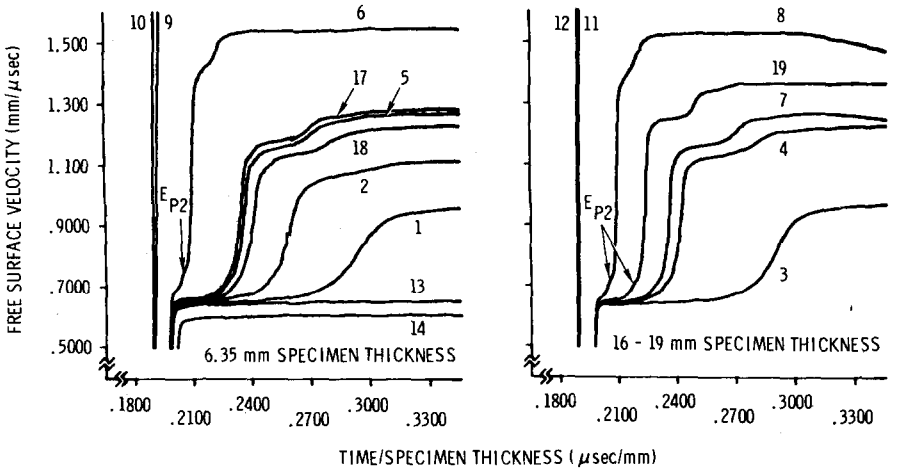

FIG. 7. Enlargements of the P2 wave portions of Fig. 3. Some perturbations (E_{P2}) which are attributed to an elastic precursor of the P2 wave are indicated.

sapphire was nearly linearly elastic in these experiments, the release wave which originated at the rear free surface of the sapphire impactor entered the iron specimen almost as a rarefaction shock. The release wave profiles of Fig. 8 thus were shaped almost entirely by the wave propagation properties of the iron. The release is not well described by an elastic perfectly plastic model since there is no two-wave structure in the release profile. A slight cusp appears at about 0.24 mm/μsec on the release of experiment 16, but there is no comparable cusp in experiment 15. An analysis of these experiments appears in Sec. IV C.

It would have been advantageous to conduct sapphire window experiments on iron at higher stress levels in order to observe the rarefaction wave profile when the reverse phase transformation, $\epsilon \rightarrow \alpha$, was known to be taking place. Unfortunately, sapphire has not yet been successfully used as a window at stresses of 15 GPa and above, and thus such experiments are precluded at present.

IV. ANALYSES AND DISCUSSIONS

The data presented in Sec. III were analyzed to extract several types of information about the dynamic behavior of iron in the 10–40-GPa stress region. In this section, we consider first the stress level at the onset of the $\alpha \rightarrow \epsilon$ phase transition. This analysis incorporates the findings on the validity of the generally assumed factor of 2 relating free-surface velocity to internal particle velocity. Second, we discuss the $\alpha \rightarrow \epsilon$ phase change relaxation time. Third, some sound speed and yield strength findings at 10 and 40 GPa will be presented. Fourth, the Hugoniot and release path calculations, and the stress at the onset of the $\epsilon \rightarrow \alpha$ reverse transformation, will be presented. Finally, we discuss the effect of a nearly saturating magnetic field on the phase transition.

A. The $\alpha \rightarrow \epsilon$ phase change stress

The free-surface velocity profiles were analyzed to find the stress level at the initiation of the $\alpha \rightarrow \epsilon$ phase change. The stress at the top of the P1 wave is identified with the onset of the phase change because it signifies a sudden increase in compressibility in the loading stress-

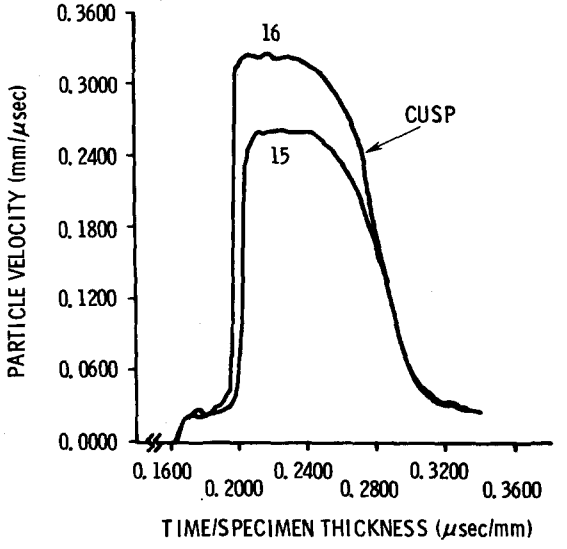

FIG. 8. Internal particle velocity histories for experiments 15 and 16. The slight cusp on the release profile of experiment 16 probably results from the reverse transformation of a small amount of ϵ-phase material back to the α phase.

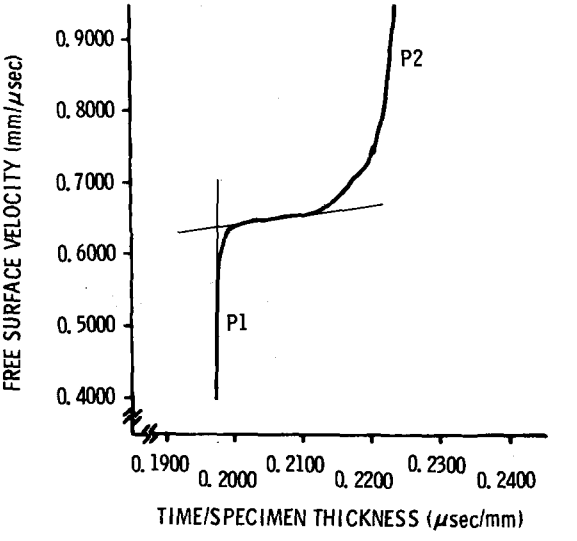

FIG. 9. Top of the P1 wave in experiment 19 illustrating the method used to define the free-surface velocity at the top of the P1 wave.

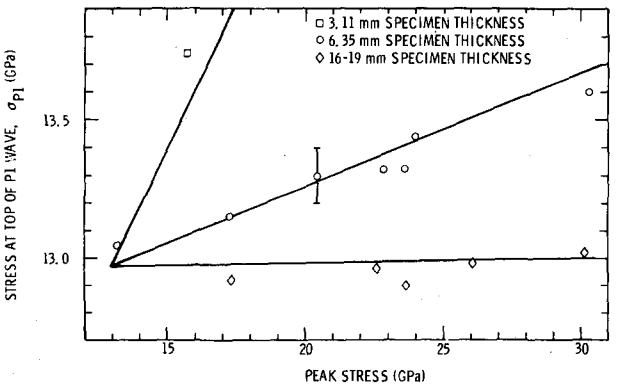

FIG. 10. Stress at the top of the P1 wave vs driving stress at impact. The error bar shown is typical of all the data points. The straight lines are fits of the data using the model of Horie and Duvall (Ref. 14). The parameter values used in the fits were 12.97 GPa for the transition stress and 0.18 μsec for the relaxation time τ.

volume curve. The transition between the very steep rise of the P1 wave and the plateau between the P1 and P2 waves is not abrupt, and the plateau is not flat. This causes difficulty in specifying a unique value for the free-surface velocity at the top of the P1 wave. The method used here is illustrated in Fig. 9. The line coinciding with the very steep rise of the P1 wave was extended upward, and a line was drawn through the plateau between the P1 and P2 waves. The intersection of the two lines was used as the free-surface velocity at the top of the P1 wave. These velocities are listed in Table I.

In order to obtain the stress and relative volume at the phase transition, one must use the Hugoniot relations

$$\Delta\sigma=\rho_0 U\Delta u,$$
$$\Delta V/V_0=-\Delta u/U. \tag{2}$$

Here $\Delta\sigma$ is the change in stress carried by the wave in question, Δu is the change in particle velocity carried by the wave, U is the Lagrangian wave velocity, ρ_0 is the initial density, V_0 is the initial volume ($V_0=1/\rho_0$), and ΔV is the change in volume carried by the wave. Equations (2) were applied first to the elastic precursor and then to the P1 wave to obtain the stress and volume at the top of the P1 wave.

An elastic wave speed of 6.00 mm/μsec was found to describe the velocity of the midpoint of the initial rise in the elastic wave. The elastic wave stress was about 1.10 GPa for the 6.35-mm specimens, and 0.92 GPa for the 16- and 19-mm specimens which agrees well with the findings of Taylor and Rice.[12] The elastic precursor in the 3.11-mm-thick specimen[17] had no overshoot in velocity, but rather a constantly increasing velocity between the elastic wave front and the P1 wave. An elastic wave stress of 1.3 GPa determined from the decay curve of Taylor and Rice[12] was assumed in the analysis of that record.

In applying Eq. (2) to the P1 wave, the measured wave velocity at the midpoint of the P1 wave front, 5.07 mm/μsec, was used. The particle velocity at the top of the P1 wave in the absence of any free-surface effects has generally been assumed to be exactly one-half of the free-surface velocity at the top of the P1 wave. However, in the present experiments we have a check on the factor-of-2 assumption because the projectile velocity was measured to an accuracy of ±0.2%. The peak particle velocity induced in the specimen, u_m, was therefore known to the same accuracy, because in symmetric impacts the particle velocity must be just one-half of the projectile velocity. The peak free-surface velocity u_{fm} was measured by the VISAR to an accuracy of ±0.3% or better. The measured values of the ratio u_{fm}/u_m are listed in Table I. These data indicate that the so-called factor of 2 is slightly less than 2.00 for iron in the range of peak stresses investigated. In particular, in the vicinity of 13 GPa, the ratio is about 1.988. However, another correction is necessary because the presence of the free surface gives rise to intramaterial interfaces,[35] and small stress-wave reflections from these interfaces delay the arrival of the final increments in free-surface velocity until well after the steep rise of the P1 wave. Whereas these late-time velocity increments are included in the tabulated values of u_{fm}/u_m, they have not yet arrived when the free-surface velocity is measured at the top of the P1 wave (Fig. 9). The magnitude of the delayed velocity increase is about 0.5%[36] and, therefore, the in-material particle velocity at the top of the P1 wave was obtained by dividing the corresponding free-surface velocity by 1.978 rather than 1.988.

The change in particle velocity carried by the P1 wave is, therefore, given by

$$\Delta u=(u_{fs}/1.978)-u_e, \tag{3}$$

where $u_e=0.0276$ mm/μsec for the 3.11-mm specimen thickness, 0.0234 mm/μsec for the 6.35-mm specimens, and 0.01953 mm/μsec for the 16—19-mm specimens. The Δu from Eq. (3) and the P1 wave speed of 5.07 mm/μsec allowed the stress and volume, σ_{P1} and V_{P1}, at the top of the P1 wave to be evaluated using Eq. (2) and the previously calculated elastic wave stress and volume. Figure 10 shows the stress at the top of the P1 wave plotted against the driving stress at impact.

B. The $\alpha\rightarrow\epsilon$ phase transformation relaxation time

It is clear from Fig. 10 that σ_{P1} is a function of both specimen thickness and the driving stress at impact, i.e., the Hugoniot stress. Also, for each group of experiments using approximately equal specimen thicknesses, σ_{P1} appears to be a linear function of the driving stress. This result is predicted by a theory of Horie and Duvall,[15] who derived an approximate equation for σ_{P1} in which they neglected yield strengths and assumed that the rate of transformation is given by

$$\frac{d\alpha}{dt}=\frac{\alpha_{eq}-\alpha}{\tau}, \tag{4}$$

where α is the fraction of the iron in the high-pressure phase, α_{eq} is the fraction which would be found in the high-pressure phase under equilibrium conditions at the given temperature and volume, and τ is a constant relaxation time. Their equation for the stress at the top of the P1 wave as a function of time is

$$\sigma_{P1}=\sigma_{P1\infty}+(\sigma_D-\sigma_{P1\infty})\exp(-t/2\tau), \tag{5}$$

where $\sigma_{P1\infty}$ is the ultimate value of σ_{P1} after a sufficiently long time and σ_D is the driving stress. If we assume the P1 wave speed to be constant, the exponential in Eq.

(5) will have the same value for all experiments with equal specimen thicknesses. Thus, σ_{P1} should be linear with σ_D, as found in Fig. 10. In fact, Eq. (5) provides a good fit of all the data, as shown by the solid lines of Fig. 10. The values of the parameters used in the fit were $\sigma_{P1\infty}=12.97$ GPa and $\tau=0.18$ μsec. In fitting the data, the attenuating time t in Eq. (5) was assumed to be only 92% of the total P1 wave transit time, for at that time the reflected E wave reduces the stress at the top of the P1 wave by about 1 GPa (cf. Fig. 5). This lowers the P1 wave stress well below $\sigma_{P1\infty}$, and thus no further decay in σ_{P1} should occur.

The analysis was repeated assuming the model of Horie and Duvall to apply only to the stress *jump* in the P1 wave. This seems consistent with the neglecting of yield strength effects in the model, and with the findings of Jones and Graham[37] that the transition stress should vary with the yield strength. Indeed, the data of Fig. 10 can be fit slightly better in this way, assuming the equilibrium stress jump across the P1 wave to be 12.00 GPa and the relaxation time to be 0.16 μsec. This result is not shown in Fig. 10 because the simpler theory falls within the error bars of all the data, with the possible exception of the 3.11-mm datum point.

The driving stress in the analysis was assumed to be equal to the equilibrium Hugoniot stress. It was pointed out by Asay[38] that the driving stress at impact should perhaps be the stress resulting from the extension of the α-phase Hugoniot into the metastable region above the equilibrium phase-transition stress. In that case, for example, the P1 wave in experiment 17 would start relaxing from a peak stress of about 28.3 GPa rather than from the Hugoniot stress of 24.0 GPa, and the relaxation time would be 0.16 μsec rather than 0.18 μsec. Fortunately, the choice of peak stress does not greatly influence the calculated value of τ.

The fitting of the data of this study by a relaxation time of 0.16–0.18 μsec appears to be in conflict with the results of a recent study by Forbes,[29] who performed shock experiments on Armco iron using a constant driving (Hugoniot) stress of about 20 GPa, and who used various specimen thicknesses down to 1 mm. Forbes observed very little decay of the P1 wave as a function of specimen thickness beyond 1 mm, and he concluded that the relaxation time is no greater than 0.05 μsec. Forbes's streak camera records do not allow measurements as accurate as ours, but his error bars account for only a small part of the discrepancy.

Although the analytical fit to the data of Fig. 10 appears to be reasonably good, the rise times of the P2 waves may not be correctly predicted by the Horie–Duvall model using a relaxation time of 0.18 μsec. Rise-time comparisons between theory and experiment with the aid of a wave propagation computer code have not been included in this paper. However, a preliminary estimate suggests that the measured rise times will lead to smaller values of τ. The peak free-surface accelerations observed during the arrival of the P2 wave are included in Table I to facilitate further investigation of the relation between the P2 wave rise times and the dynamics of the $\alpha \rightarrow \epsilon$ phase transition.

There is one final bit of evidence which suggests that the relaxation time of 0.18 μsec does not explain all of the observed behavior. Recall it was assumed the velocity of the P1 wave is constant regardless of the driving stress. However, if the P1 wave loads the iron to a metastable point on the extension of the α-phase Hugoniot, the instantaneous velocity of the P1 wave should be a function of the instantaneous stress at the top of the P1 wave, with higher stresses producing higher wave velocities. Therefore, those experiments with the highest driving stresses should have the highest average velocities of the P1 wave. This effect should be noticeable in the time difference between the free-surface arrivals of the elastic precursor and the P1 wave: the difference in arrival times should be less for the higher driving stress experiments. This assumes, of course, that the elastic precursor velocity is independent of the driving stress.

An estimate was made of the expected magnitude of this effect by assuming the linear U-u relation for α-phase iron below 13 GPa also describes the wave velocity at metastable α-phase states above 13 GPa. Using $\tau=0.18$ μsec, the average P1 wave velocity should have been about 3% higher in experiment 6 than in experiment 13. However, a close examination of the elastic wave and P1 wave separations indicates the P1 wave velocity of experiment 6 was higher by less than 1%. This would indicate a relaxation time τ of 0.06 μsec or less, which is in agreement with the conclusion of Forbes.[29]

Various aspects of the present data seem to indicate different values for the relaxation time. These discrepancies may indicate that a model assuming a single constant relaxation time is too simple to provide a good general description of the phase transition in iron.

C. Release wave speeds and yield strengths

Experiments 15 and 16 of this series provide very good measures of the initial release wave speeds from peak stresses of 10.3 and 13.2 GPa in α-phase iron. Likewise, experiments 11 and 12 provide good measures of the release wave speeds from nearly 40 GPa in ϵ-phase iron. These four experiments also tell us something about the yield behavior of iron at high pressure. This section considers first the α-phase data of experiments 15 and 16, after which the ϵ-phase data of experiments 11 and 12 are analyzed.

As indicated in Table I, experiments 15 and 16 consisted of sapphire driver plates impacting the iron specimens, with sapphire windows on the rear surface of the specimens through which the VISAR recorded the motion of the iron-sapphire interface. The sapphire was nearly linearly elastic in the stress range of these experiments, and thus, to a good approximation, the impactor introduced a step-function compression followed by a step-function release.

The time of the initial release at the impact surface of the specimen was calculated using an equation of state for the sapphire driver plate consistent with the linear U-u relation

$$U=C_0+Su, \tag{6}$$

with $C_0=11.19$ mm/μsec and $S=1.0$.[23] Since the sapphire window on the specimen rear surface had a shock

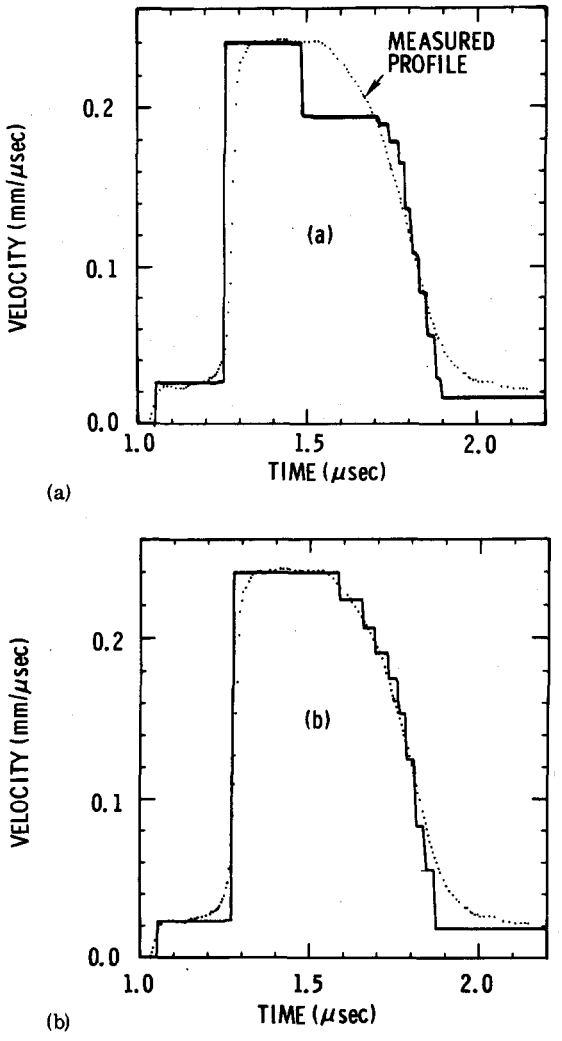

FIG. 11. Comparison of measured and calculated profiles for experiment 15. The computed profile in (a) assumed elastic perfectly plastic behavior; (b) incorporates a decreasing yield strength, Bauschinger effect, and increasing Poisson's ratio with increasing compression.

impedance only slightly greater than that of iron, the wave reflected back into the iron from the iron-sapphire interface was a small recompression of less than 1 GPa. The release wave traversed more than 85% of the specimen thickness before encountering the slightly higher stress level due to the iron-sapphire interface reflection. Accordingly, the release wave speed through the iron was assumed to be constant. The Lagrangian wave speeds of the initial release were thus found to be 6.36 mm/μsec at 10.26 GPa for experiment 15, and 6.40 mm/μsec at 13.15 GPa for experiment 16.

In order to evaluate the yield behavior of iron at about 10 GPa, the velocity profile of experiment 15 was calculated using the rate-independent SWAP-9 code.[39] A comparison of calculated and measured profiles appears in Fig. 11. Equation (6) with $C_0 = 4.63$ mm/μsec and $S = 1.33$ was used to describe the shock hydrostat of iron in Fig. 11(a), along with a constant yield strength of 0.7 GPa and a constant Poisson's ratio of 0.285, which is the ambient value. Although the elastic precursor is well approximated, the calculated initial elastic release arrives too early and is much too large. To achieve the good release wave fit of Fig. 11(b), the yield strength in the calculations was made a decreasing function of the compression, such that the compressive yield strength began at 0.65 GPa at zero stress and decreased to 0.32 GPa at the peak stress of 10.26 GPa. In addition, a large Bauschinger effect was assumed in which the yield strength in tension was zero at the start of the release, but increased exponentially with plastic deformation during the release toward the value of the compressive yield strength. Finally, the calculated profile of Fig. 11(b) assumed Poisson's ratio increased with increasing compression, starting at 0.285 and reaching a value of 0.388 at 10.26 GPa. This latter assumption was found necessary to decrease the elastic wave velocity so as to match the observed arrival time of the release wave.

It is apparent from Fig. 11 that the yield strength behavior is quite different from an elastic perfectly plastic model. The decrease in yield strength and the large apparent increase in Poisson's ratio which were found to fit the data show a tendency toward hydrostatic behavior. In fact, a hydrostatic model fits the release profile of experiment 15 at least as well as the elastic perfectly plastic profile of Fig. 11(a).

In the following, we wish to discuss the release wave profile of experiment 15 in greater detail. To that end, the Armco iron Hugoniot below 13 GPa will first be reviewed, and from the Hugoniot and Grüneisen's parameter we shall estimate the bulk wave velocity at 10.26 GPa. The bulk velocity and the velocity of the first detectable release allow the calculation of Poisson's ratio. We shall then present arguments to the effect that perhaps *no* part of the observed release wave is representative of purely elastic behavior.

The bulk wave velocity in Armco iron at room temperature and pressure is $C_0 = 4.63$ mm/μsec.[40] The P1 wave velocity at 13 GPa was determined to be 5.07 mm/μsec as indicated in Sec. II. Thus, a linear U-u estimate of the α-phase shock hydrostat, assuming a constant yield strength, is

$$U = 4.63 + 1.33u \quad \text{mm/μsec}, \tag{7}$$

as already assumed in the computer fits of Fig. 11. This relation is in good agreement with our measurements on experiments 14 and 15, and in good agreement with measurements by Taylor and Rice[12] when it is recognized that those authors reported velocities of the toe of the P1 wave rather than the midpoint of the wave front.

By using Eq. (7) for the shock hydrostat and assuming a constant Grüneisen parameter of 1.7, one finds[41] that the bulk wave velocity at 10.26 GPa is $C_B = 5.32$ mm/μsec. The bulk velocity and the measured initial release velocity, $C_E = 6.36$ mm/μsec, can be used to calculate Poisson's ratio from

$$\nu = (3C_B^2 - C_E^2)/(3C_B^2 + C_E^2). \tag{8}$$

The result is $\nu = 0.355$, which is a rather surprising increase over the zero pressure value of 0.285. Taylor and Rice[12] noted qualitatively the same result, stating that the initial rarefaction seemed always to travel at approximately the elastic precursor velocity regardless of the peak stress level (up to 8 GPa).

It is interesting to note there is no indication of a *finite purely elastic* stress range in the release profile

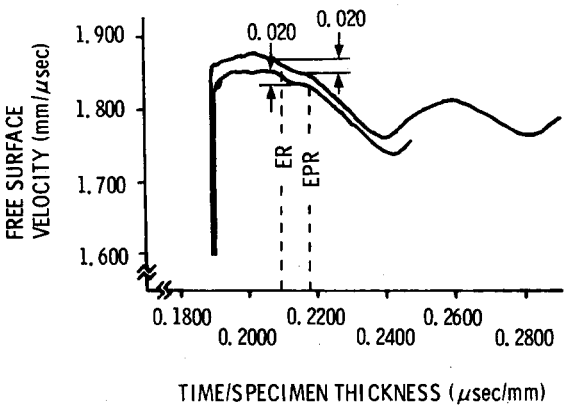

FIG. 12. Enlargements of the free-surface velocity histories of experiments 11 and 12 during the release wave arrivals. ER and EPR are release wave arrivals; the origins of the waves are shown in Fig. 13.

of experiment 15. If there had been such a stress range, the initial part of the release wave profile should have been much steeper than was measured, and should have flattened out somewhat before resuming the steep slope of the plastic release. The shallow initial slope of the release indicates that no part of the release wave, save perhaps the very first increment of particle velocity decrease, travels with the purely elastic wave velocity.

Since it seems clear that only the velocity of the very start of the release could be indicative of purely elastic behavior, and since the first observable release travels with a velocity which implies a large increase in Poisson's ratio, one might speculate that even the velocity of the initial release is not indicative of purely elastic behavior. A large amount of twinning,[33] dislocation multiplication, and dislocation motion are required to accomodate the large and extremely rapid uniaxial strain deformation in the P1 wave. The material behind the P1 wave might be in a chaotic state from which it must self anneal before it can display the same elastic effects which would be observed in a quasistatic experiment.

We now turn to a discussion of the release wave behavior at nearly 40 GPa. Figure 12 shows an enlargement of the release wave portions of the free-surface velocity profiles of experiments 11 and 12. These experiments were nearly identical, consisting of 6.33-mm-thick Armco iron driver plates impacting 19.1-mm-thick specimens to create peak stresses of nearly 40 GPa. The driver plates were supported by thick 6061-T6 aluminum disks to prevent any distortion of the plates during the projectile's acceleration down the barrel of the gun.

The initial decrease of 0.02 mm/μsec in free-surface velocity at ER in Fig. 12 appears to preceed the main part of the free-surface velocity decrease. This early rarefaction wave arrival has the correct amplitude to identify it as the result of the early partial reflection of the elastic precursor from the iron-aluminum interface in the impactor, as illustrated in the x, t diagram in Fig. 13. The main part of the free-surface velocity decrease begins at EPR in Fig. 12, and that wave originates with the partial reflection of the P2 wave from the iron-aluminum interface. The Lagrangian velocity of the center of the ER wave front was calculated to be 8.98 ± 0.10 mm/μsec. The calculation used 6.00 mm/μsec as the velocity of the center of the initial rise of the elastic precursor wave front, and 5.0 mm/μsec as the velocity through the material at zero stress next to the free surface (Fig. 13). One might have assumed the plastic wave velocity of 4.63 mm/μsec instead of 5.0 next to the free surface, but there is strong evidence that materials tend to propagate a reloading in the same direction as a previous loading at higher than the bulk wave velocity.[23,42,43] In any case, the elastic wave velocity at 39.5 GPa is not sensitive to the velocity assumed for the ER wave near the free surface because that velocity prevails for only a few percent of the transit time.

The Lagrangian velocity of the EPR wave was calculated using a similar approach and was found to be 8.85 ± 0.10 mm/μsec. Note that the iron into which the EPR wave travels has just been released by about 0.7 GPa by the ER wave. The continued quasielastic release wave velocity after a 0.7 GPa release shows that the yield strength of the iron at 40 GPa on the Hugoniot is not insignificant. However, as with the release from 10 GPa in experiment 15, there is no clear breakpoint on the release wave profile other than that caused by the early reflection of the ER wave. The velocity seems to gradually change from the elastic to the bulk value with continuing rarefaction.

The acceleration reversals in the free-surface velocity profiles of Fig. 12 at about 0.24 scaled time are caused by a spallation in the iron near the free surface. The portion of the release wave which arrives at the free surface at the time of the acceleration reversal has a velocity of about 7.63 mm/μsec in the ϵ-phase iron. This velocity is probably fairly close to the isentropic bulk velocity, since calculating the bulk velocity from the slope of the Hugoniot[44] and assuming a Grüneisen parameter of 2.0 gives a value of 7.45 mm/μsec at a Hugoniot stress of 40 GPa. The peak stress has been released by about 3.5 GPa in the material through which the local release wave velocity is 7.63 mm/μsec. The situation in experiment 15 was quite similar: after a re-

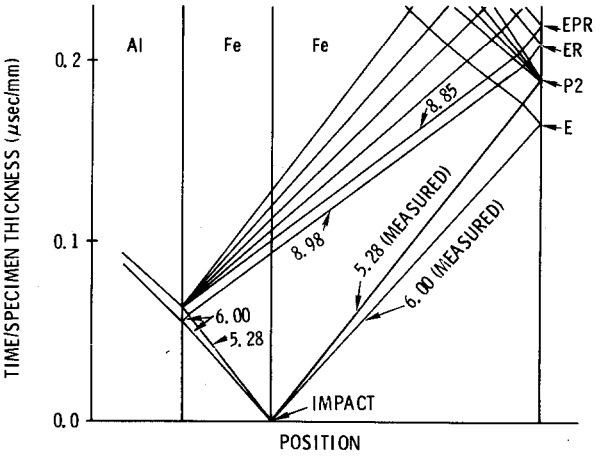

FIG. 13. The x,t wave propagation diagram for experiments 11 and 12. Some of the wave velocities are shown. E denotes the free-surface arrival of the elastic precursor, P2 is the arrival of the phase transition wave, ER is the first elastic release, and EPR is the arrival of the release which originated at the partial reflection of the impactor's P2 wave from the iron-aluminum interface.

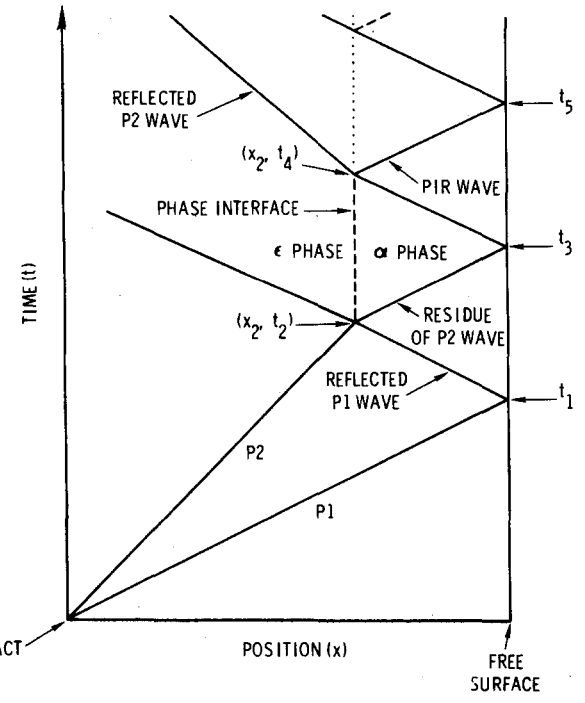

FIG. 14. Illustrative x,t diagram of stress wave propagation in iron. The elastic waves have been omitted here for simplicity.

lease of 3.5 GPa, the local release wave speed was close to the isentropic bulk wave speed. It, therefore, appears the yield strength behavior of ϵ-phase iron at 40 GPa is quite similar to α-phase iron at 10 GPa. If the calculated bulk wave velocity of 7.45 mm/μsec is correct, that value and the initial release wave speed of 8.98 mm/μsec give a Poisson's ratio of 0.347 at 40 GPa in ϵ-phase iron.

Al'tshuler *et al.*[45] experimentally determined an Eulerian elastic release wave speed of 7.15 mm/μsec at a Hugoniot stress of 41.5 GPa. This translates into a Lagrangian wave speed of 8.75 mm/μsec, compared to our value of 8.98 mm/μsec at 39.5 GPa. The agreement is gratifying, considering that Al'tshuler's data were obtained from the velocities of edge effects into the region of uniaxial strain in plate impact experiments. Al'tshuler *et al.*[45] also measured the isentropic bulk velocity using an overtaking rarefaction wave technique. They obtained an Eulerian speed of 7.51 mm/μsec. This is in excellent agreement with the isentropic bulk speed of 7.45 mm/μsec at 40 GPa calculated from the Hugoniot slope and an assumed Grüneisen parameter of 2.0.

The initial release wave arrival at the free surface was recorded in at least 14 other experiments which have not been discussed in this section. In most cases, the initial release originates with the reflection of the elastic precursor from the back surface of the driver plate, while in other experiments the first observed release originates with the peripheral edge effects. The analysis of the release wave behavior in these 14 experiments is more complicated than in the four experiments discussed above, and any one experiment can give ambiguous results because no single release velocity plays a predominant role in determining the arrival time. Nevertheless, it should be possible to develop a consistent model to explain the observed release wave behavior. Such a study is beyond the scope of this paper.

D. Loading and unloading stress-volume paths

It can be seen from Fig. 8 that experiment 16 has a slight cusp in its rarefaction wave profile well down from the peak particle velocity. The cusp is thought to be related to the $\epsilon \rightarrow \alpha$ reverse phase transformation. The peak impact stress of experiment 16, 13.15 GPa, is just slightly greater than the equilibrium $\alpha \rightarrow \epsilon$ phase transition stress, and thus a small fraction of the iron should transform into the ϵ phase. Also, as previously mentioned, the interaction of the P1 wave with the iron-sapphire interface produces a reflected wave which further increases the stress in the iron close to the interface by about 1 GPa before the release wave arrives. Thus, the portion of the material which transformed to the ϵ phase must retransform back to the α phase as the stress is relaxed. It has been known for some time that the release wave in iron forms a shock as a result of the $\epsilon \rightarrow \alpha$ reverse transformation.[46,47] The sudden steepening of the release wave at the cusp in experiment 16 is, therefore, interpreted as a slight tendency toward the formation of a rarefaction shock because of the $\epsilon \rightarrow \alpha$ transformation of the small fraction of the specimen which was transformed into the ϵ phase. The position of the cusp on the release wave profile indicates the reverse transformation takes place well below the 13.15-GPa peak impact stress.

The observed final increase in free-surface velocity, i.e., the PIR waves of Fig. 2 and 3, can also be satisfactorily explained by supposing that the reverse phase transformation occurs at a substantially smaller stress level than the forward transformation. Referring to the x,t wave diagram of Fig. 14, the P1 wave reaches and reflects from the free surface at time t_1. The 13 GPa relaxation carried by the reflected P1 wave then encounters the oncoming phase transition (P2) wave at coordinates (x_2, t_2), where it decreases the peak stress behind the P2 wave by some 13 GPa. Let us assume, for example, that the residual stress behind the P2 wave after the interaction is only 10.5 GPa. Since the material next to the free surface through which the oncoming residue of the P2 wave is now traveling has never experienced a stress above 13 GPa, it remains in the α phase. However, after time t_2 the reflected P1 wave is traveling into ϵ-phase material and reducing the stress to 10.5 GPa. If the iron remains in the ϵ phase on release to 10.5 GPa, there will exist, after time t_2, a boundary at x_2 between the α and ϵ phases: material to the left of x_2 will remain (for the moment) in the ϵ phase, and material to the right of x_2 will remain in the α phase. This interface, or contact discontinuity, will perturb other waves reaching the x_2 plane, and is the source of the PIR wave as described below.

At time t_3, the residue of the P2 wave reflects from the free surface. The resulting 10.5-GPa release wave then encounters the interface between the α and ϵ phases at x_2. As the release wave enters the ϵ-phase material, that material's stress-volume release path must be much less steep than the stress-volume release path for the α material in order to accomplish the now mandatory reverse phase transformation. The result is a mismatch of material properties at x_2, such that part of the 10.5-

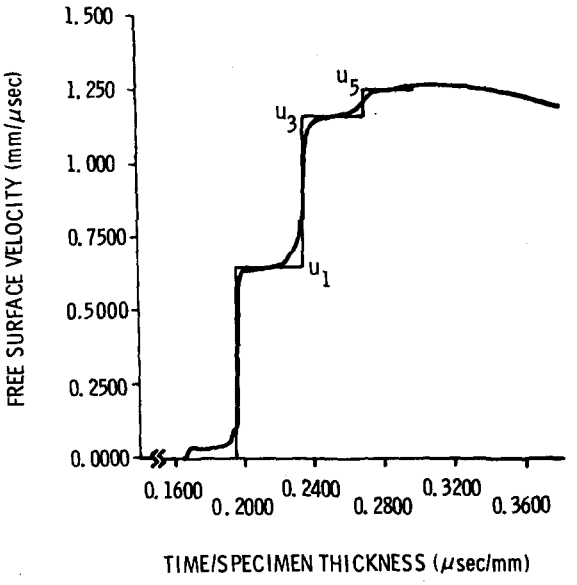

FIG. 15. Illustration of the stepwise approximation of the free-surface velocity used in the calculation of loading and unloading stress-volume paths.

GPa release wave is reflected back toward the free surface as a recompression. Since the wave velocities in the α phase of iron do not vary drastically with stress level or loading direction, it is seen from Fig. 14 that the phase interface reflection (PIR wave) should arrive at the free surface at a time which is roughly equal to $t_5 = t_3 + (t_3 - t_1)$. This time agrees with the experimentally observed arrival time of the final increase in free-surface velocity. This explanation of the origin of the PIR wave will be further strengthened in the following calculation of the loading-unloading stress-volume path.

Since the iron to the right of x_2 in Fig. 14 never transforms into the ϵ phase, we can perform an analysis in which we make use of the known properties of this always α material. For each experiment, these properties and the measured free-surface motion allow us to determine two or three points on the release path of the iron exposed to the peak shock stress. The combined results of the experiments then clearly outline the entire release behavior.

The analysis makes use of the fact that the impactor plates and the specimen plates were both made of iron, so that the input particle velocity at the impact plane was just one-half of the measured impactor velocity. Several simplifying approximations are made in order to reduce the analysis to a tractable process. The approximations include (i) using the factor-of-2 assumption to relate internal particle velocity to free-surface velocity for the α iron, (ii) accounting for elastic-plastic effects in the α iron only by weighting the plastic wave speeds according to the relative amplitudes of the elastic and plastic portions of the wave, (iii) approximating the free-surface velocity profiles as a series of discontinuous increases in velocity, with constant velocity regions separating the discontinuities (Fig. 15), and (iv) assuming each of the wave velocities to be constant. In each reworked profile the P1 wave was the first jump in velocity, followed by the P2 wave, and then the phase interface reflection. In most cases there was an additional late-time small increase in free-surface velocity after the arrival of the phase interface reflection. This was considered to be a second reflection from the location of the formerly existing phase interface.

With these approximations, the stress-volume behavior was calculated with reference to the x, t plane (Fig. 14) and the σ, u plane (Fig. 16). The conventional shock jump relations were used [cf. Eq. (2)].

The Δu carried by the P1 wave was taken as one-half the free-surface velocity u_1, following the P1 wave arrival at the free surface (see Fig. 16). The actual wave velocity of the P1 wave was increased slightly (about 1%) by a weighting factor in the analysis to account for the fact that the elastic precursor was not included explicitly. The resulting U and the $\Delta u = \frac{1}{2}u_1$ were then used in Eq. (2) to obtain the stress and volume behind the P1 wave.

Next, the Δu and U for the P2 wave are required in order to calculate the final Hugoniot stress and volume of the experiment. The Δu is simply $\frac{1}{2}(u_{imp} - u_1)$, where u_{imp} is the impactor velocity. In order to obtain U for the P2 wave, we refer again to the x, t diagram of Fig. 14. Let the velocity of the reflected P1 wave be assumed equal to the incident P1 wave velocity. Also, from Eq. (7) the velocity of the residue of the P2 wave is known. Thus, knowing these two wave velocities and the times t_1 and t_3, one can calculate the wave interaction coordinates (x_2, t_2). The desired Lagrangian shock velocity of the P2 wave is then simply $U = x_2/t_2$. Thus, the change in stress and volume carried by the P2 wave can be calculated. The final Hugoniot stress in the experiment is then equal to the stress behind the P1 wave plus the change in stress carried by the P2 wave, and likewise for the volume.

We now wish to calculate the stress σ_r and particle velocity immediately behind the residue of the P2 wave (Fig. 14). When that wave reaches the free surface, the free-surface velocity increases from u_1 to u_3 (Fig. 16). Using the factor-of-2 approximation, the particle velocity behind the wave is $u = \frac{1}{2}(u_1 + u_3)$, and the change in

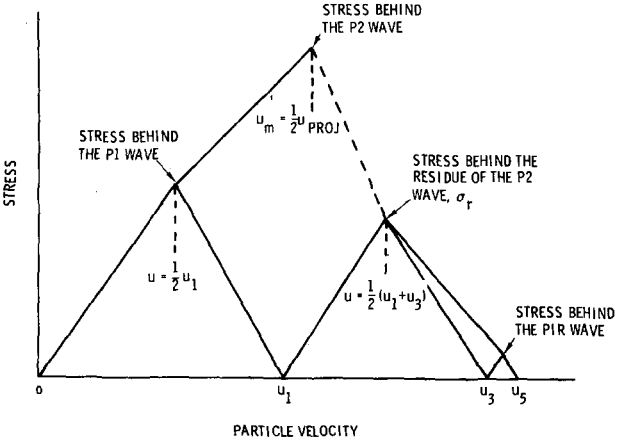

FIG. 16. Stress vs particle velocity plot used in solving for the loading and unloading stress-volume paths. The slope from the P1 to the P2 stress is smaller than from the P2 to the σ_r stress because only the P1 to P2 path involves a complete change of phase. The reverse phase change occurred primarily between the σ_r and PIR stresses.

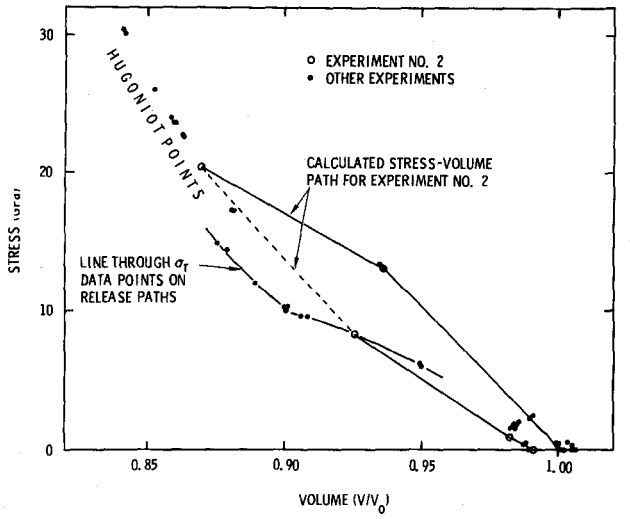

FIG. 17. Loading and unloading stress-volume points obtained in the preliminary analysis of the free-surface velocity profiles.

particle velocity carried by the wave is $\Delta u = \frac{1}{2}(u_3 - u_1)$. As discussed previously, the residue of the P2 wave travels in purely α-phase iron, and we assume U is known as a function of Δu for α iron. Thus, both U and Δu for the residue of the P2 wave are known, and the stress behind the wave, σ_r, can be found from Eq. (2). The resulting stress and particle velocity point are shown in Fig. 16.

Referring back to Fig. 14, we have just calculated the stress and particle velocity in the α material immediately to the left of the residue of the P2 wave. However, both stress and particle velocity are continuous across interface boundaries, and therefore, the same stress and particle velocity exist in the ϵ-phase iron to the left of the phase interface at x_2. Recall also, we have already calculated the peak stress and the particle velocity to the left of the P2 wave. Thus, the stress and particle velocity are known both ahead of and behind the reflected P1 wave which travels into the ϵ-phase iron after the interaction at (x_2, t_2). Knowing the changes in stress and particle velocity for that wave allows one to solve the first part of Eq. (2) for the wave velocity U, and hence $\Delta V/V_0$ can also be found from the second part of Eq. (2). Thus, a stress-volume point at σ_r on the release path of the material exposed to the peak stress of the experiment has been calculated. The σ-u behavior during the release by the reflected P1 wave is indicated by the dashed line in Fig. 16.

We can calculate another stress-volume point on the release path by a similar analysis of the change in free-surface velocity produced by the phase interface reflection. If the free-surface velocity after the arrival of the PIR wave is u_5, the particle velocity behind the wave is $\frac{1}{2}(u_3 + u_5)$, and the change in particle velocity is $\Delta u = \frac{1}{2}(u_5 - u_3)$. Using Δu and the known properties of α iron, U is obtained and the stress behind the PIR wave is found from Eq. (2). From these calculations we know the stress and particle velocity to the left of the phase interface reflection in Fig. 14; the same stress and particle velocity must be present to the left of the phase interface location at x_2 (the dotted line in Fig. 14). Thus, the stress and particle velocity are known both ahead of and behind the reflected P2 wave to the left of x_2. The changes in stress and particle velocity can then be used in Eq. (2) to solve for U and to find $\Delta V/V_0$. This calculation provides a second point on the release path of the iron. In most of the experiments, a small late-time increase in free-surface velocity was observed after the arrival of the PIR wave. This was assumed to be still another reflection from the boundary at x_2 and was analyzed accordingly.

Figure 17 shows the stress-volume points obtained from the preliminary analysis, as outlined above. The stress-volume points for experiment 2 have been connected by lines to show the stress-volume history during the experiment. The dashed unloading line from the Hugoniot point to the first data point on the release path corresponds to the dashed unloading path in Fig. 16. Experiments 1–8 and 17–19, inclusive, each gave a similar stress-volume path, contributing one data point each to the early part of the release. The other experiments did not contribute to the release path information, and are not shown in Fig. 17.

The Hugoniot points of Fig. 17 show very little scatter between the 6.35-mm and the 16–19-mm data. This attests to the accuracy of the assumption of constant compressive wave velocities. Likewise, the release stress-volume points are initially quite consistent, but there is a scatter of about ± 0.009 in the residual relative volume after unloading is complete. The release path data of Fig. 17 show a well-defined cusp at about 10 GPa. The cusp is interpreted as the initiation of the $\epsilon \rightarrow \alpha$ reverse phase transformation, with the consequent rapid increase in volume as the stress is decreased. Since it occurs at about 10 GPa and, whereas the forward $\alpha \rightarrow \epsilon$ transformation occurs at about 13 GPa, these results are consistent with our previous hypothesis of a hysteresis in the phase transformation.

The analysis leading to Fig. 17 used the assumption that the unloading path from the peak stress (the Hugoniot point) to the stress behind the residue of the P2 wave (σ_r) was a straight line on the σ, u plane, as indicated by the dashed line in Fig. 16. This also maps into a straight line release between these two stresses on the σ, V/V_0 plane, as shown in Fig. 17. The straight-line approximation may be reasonably good for those experiments in which σ_r is very close to the start of the reverse phase transformation. However, when the σ_r point for the experiment was appreciably lower than about 10 GPa (as was the case for experiment 2), it can be seen from Fig. 17 that the straight-line release is a poor approximation if the release path in reality passes through the reverse phase transformation point at the cusp in the line connecting the σ_r data points.

An improved analysis of the data was, therefore, made using the information gained in the preliminary analysis described above. The release path was always forced through the reverse phase transition point, which was chosen as 9.8 GPa at a relative volume of 0.903 for an experiment with a peak stress of 23.0 GPa. The "standard" reverse transition volume of 0.903 was then adjusted slightly for each experiment by taking into account the difference in internal energy at 9.8 GPa compared to the standard 23.0-GPa experiment. A

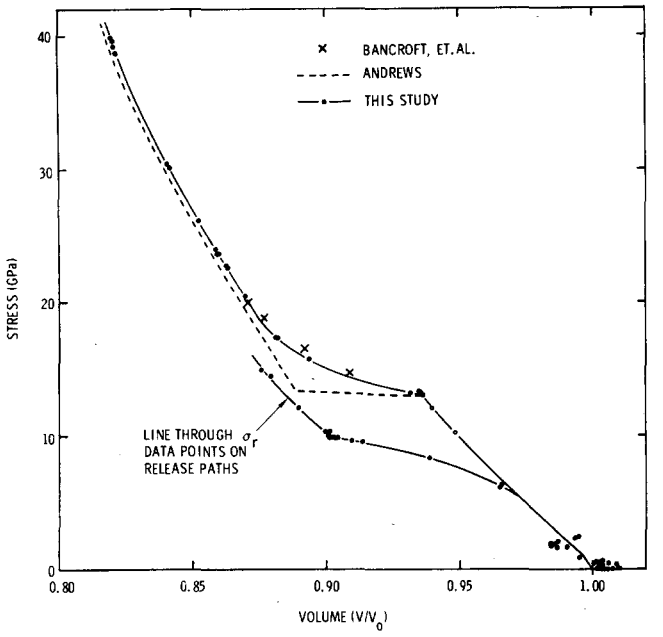

FIG. 18. Hugoniot and unloading stress-volume data. The many data points in the lower right-hand corner represent the terminations of release paths obtained from the data. The dashed line is the thermodynamically consistent Hygoniot calculated by Andrews (Ref. 49) from a variety of experimental data.

Grüneisen parameter of 2.00 was used. In addition, a realistic curvature was put into the release path from the Hugoniot point down to the greater of σ_r or 9.8 GPa. This was intended to approximate the actual release adiabat, whose curvature was undoubtedly accentuated by the presence of quasi-elastic-plastic effects, as were present at 40 GPa. However, it was found the results of the analysis were not very sensitive to the degree of curvature assumed.

With these improvements, the analysis provided the stress-volume plot of Fig. 18 which includes the Hugoniot points of all of the experiments of this study. The scatter in the residual volume after unloading has been reduced to ± 0.005 by the improved analysis, and if the differences in internal energies are taken into account, the effective scatter is only ± 0.0033. Also, after correcting the volumes for the increase in internal energy, the average residual relative volume was 0.9995.

When the unloading paths are forced through the reverse phase transition point, the data points just below the transition are moved to the right by a substantial amount. This serves to accentuate the cusp in the release stress-volume path even more than in the preliminary analysis shown in Fig. 17. The reverse phase transition stress of 9.8 GPa was chosen because several experiments with σ_r points at 10.0 GPa and above showed no break in the release path, while two experiments with $\sigma_r \approx 9.6$ GPa were offset in the larger volume direction.

The experiments whose σ_r's closely bracket the 9.8 GPa reverse phase transition point all have peak impact stresses in the vicinity of 23 GPa. Therefore, the specimen temperature at the reverse transition point was always approximately the same in these particular experiments. However, different peak stress levels produce different entropy increases, and therefore different temperatures at the reverse transition point. Since the reverse transition stress level is undoubtedly a function of the temperature, the value 9.8 GPa is strictly valid only for a temperature of about 350 K, which is the temperature at the reverse transition for a 23-GPa peak stress shock experiment starting at 295 K.[48] If the phase line for the $\epsilon \rightarrow \alpha$ reverse transition has the same slope as for the $\alpha \rightarrow \epsilon$ forward transition, shock experiments starting at room temperature may have reverse phase change stresses which decrease by about 0.5 GPa as the peak stress in the experiment is raised from 20 to 30 GPa. However, no variation in the reverse transition stress was assumed in the data analysis which led to the release stress-volume path indicated in Fig. 18. The effect of assuming the same phase line pressure-temperature slope as the forward transition would be quite small and of doubtful value without further information.

The present experiments show that there is no pronounced indication of rate effects in the observed reverse phase change, because the small family of experiments which define the 9.8-GPa reverse phase change stress is composed of both 6.35-mm specimens and 16—19-mm specimens. In fact, both thicknesses have σ_r points which just bracket the 9.8-GPa level, and both are consistent with the 9.8-GPa value. Since the unloading sequence is $2\frac{1}{2}$—3 times slower in the 16—19-mm specimens, rate effects are not evident in these experiments. On the other hand, the reverse transformation could be no faster than the forward one and still show no effects here.

It is difficult to determine limits of accuracy in an analysis such as this. The measured wave profiles were "squared off" for the analysis, only cursory attention was given to elastic-plastic effects, and rate effects were not included. Nevertheless, the loading and unloading stress-volume paths were probably approximated quite well by including curvature in the initial unloading, by forcing the unloading paths through the 9.8-GPa reverse phase transition point and by allowing the volume at the reverse transition to vary with internal energy. The relatively small scatter of residual volumes and the negligible average net change in volume except for thermal expansion seem to indicate the analysis is reasonably accurate. From these considerations it is estimated that the reverse phase transition stress of 9.8 GPa at a temperature of 350 K is accurate to within ± 0.4 GPa.

The data of Bancroft *et al.*[1] shown in Fig. 18 were obtained about 20 years ago using explosively generated attenuating wave fronts and electrical pin contactors to measure the free-surface displacement history. It is to their credit that with nonattenuating plate impact-generated waves and with much more sophisticated free-surface velocity instrumentation we can suggest only minor changes to their measured Hugoniot. Our data fall slightly below theirs in the mixed phase region between 13 and 17 GPa. However, our data are still much higher than the almost constant-stress mixed phase region of the equilibrium Hugoniot calculated by Andrews.[49] This indicates the transition does not go to completion in the time scale of shock experiments unless the peak stress is several GPa above the 13 GPa calculated by Andrews[49] as the Hugoniot stress for complete transition.

An apparent reluctance of the phase transition to go to

completion has also been found in several quasistatic high-pressure investigations. For example, Giles *et al.*[19] measured the onset of the transition at 13.3 GPa, but estimated that 40% of the α phase was still present at 16.3 GPa. On the other hand, the data of Takahashi *et al.*[20] indicate the onset at 12.9 GPa and completion at about 16.3 GPa. Our Hugoniot would suggest about 15% α phase still present at 16.3 GPa.

The present work is the first shock wave study to provide a measure of the stress level at the onset of the reverse phase transition in iron. Our value of 9.8 ± 0.4 GPa falls within the error bars of the 8.1 ± 1.7 GPa estimate of Giles *et al.*[19] who based their figure on their observation of no reverse transition at 9.8 GPa but some reverse transition at 6.6 GPa. Takahashi *et al.*[20] indicate 6.0 GPa as the onset of the reverse transition, but they do not state the accuracy of their measurement.

A strong case is made by Giles *et al.*[19] for the martensitic nature of the $\alpha \rightleftharpoons \epsilon$ phase transition, based in part on the reluctance of the transition to go to completion and on the hysteresis in the forward and reverse phase changes. The results of the present work are consistent with these findings.

E. Effect of a magnetic field on the phase transition

It was pointed out by Curran[18] that the $\alpha \rightarrow \epsilon$ phase transition includes a magnetic transition because the ϵ phase is not ferromagnetic,[50,51] and therefore the phase-transition stress should depend on the applied magnetic field because of the magnetic Gibbs energy of α iron. Curran's analysis indicated that a magnetic field should shift the phase transition slightly toward a higher stress. However, Curran and Hornemann[52] calculated that the magnitude of the stress change should be of the order of 10^{-4} GPa, and therefore unobservable in a shock experiment.

A number of experiments were performed by Curran[18] on Armco iron which was magnetized to near saturation. A decaying shock was introduced into the specimen, and the propagation distance at which the wave decayed to below the phase transition stress was measured. This was done by a postmortem cross sectioning and etching of the sample. The portion which had undergone the phase transition etched to a different shade than the untransformed material. As a result of these experiments, Curran concluded that the phase-transition stress decreased by about 1 GPa instead of remaining essentially constant, as predicted by theory.

In view of the discrepancy between theory and experiment, it seemed advisable to confirm Curran's experimental result by the techniques of the present study, i.e., by measuring the free-surface velocity profile to determine the stress at the top of the P1 wave in essentially magnetically saturated Armco iron specimens. This was done in experiments 17 and 18. The specimens were magnetized by placing a 2000-G permanent horseshoe magnet on the free surface of the specimen. The wave propagation was observed at the midpoint between the poles of the magnet.

The free-surface velocity profiles of experiments 17 and 18 are plotted with the profiles of the unmagnetized specimens in Sec. III of this paper. The calculated stresses at the tops of the P1 waves are tabulated in Table I and are plotted along with the unmagnetized specimen data in Fig. 10. In fact, the data from experiments 17 and 18 have been included with the data of the rest of the experiments in all of the foregoing analyses of the data, and in every case the magnetized specimen data fit in perfectly with the unmagnetized specimen data. It is felt that an effect on the phase-transition stress as small as 0.1 GPa would have been detected in this study. Thus, the present results contradict Curran's measurements, but agree with Curran and Hornemann's[52] theory.

V. CONCLUSIONS

The generally assumed factor of 2 relating the peak free-surface velocity to the peak particle velocity in plate impact experiments has been found experimentally to hold to within about 1% for iron, provided sufficient free-surface observation time is allowed to include relatively late-arriving final increments in velocity. However, care must be exercised in using the factor of 2 to determine the particle velocity change carried by the P2 wave, for the Δu of the P2 wave internal to the iron is divided between the P2 and PIR increases in free-surface velocity (cf. Fig. 2). Serious errors in particle velocity can result if insufficient observation time is allowed to include the PIR wave in the Δu assigned to the P2 wave internal to the iron. Fortunately, appreciable errors in particle velocity produce only small errors in the location of the Hugoniot. This may account in part for the relatively good agreement between the Hugoniot of this work and the Hugoniot points of Bancroft *et al.*[1]

The equilibrium value for the onset of the $\alpha \rightarrow \epsilon$ phase transition[53] which produces a best fit with the phase-transition rate model of Horie and Duvall[15] was 12.97 GPa. However, the 16–19-mm specimen data seem to point to an equilibrium value of 12.88 GPa, while the 6.35-mm specimen data are best fit by a value of 13.03 GPa. Thus, it seems the stress at the top of the P1 wave continues decaying slowly, as found by Minshall,[9] possibly as a result of the continuing slow decay of the elastic precursor, as suggested by Forbes.[29] The present data, therefore, seem to indicate the equilibrium $\alpha \rightarrow \epsilon$ phase-transition stress for shock experiments is about 12.8 ± 0.1 GPa for as-received Armco iron.

Assuming the model of Horie and Duvall,[15] a relaxation time of 0.18 μsec produces a good fit of the P1 wave amplitude data for the experiments of this study, but the same relaxation time also predicts a much larger variation in the average P1 wave velocity than was observed. It appears that the simple model of Horie and Duvall may not be sufficient to explain all aspects of the experimental data.

The release wave profiles for α-phase iron indicate either a strong increase in Poisson's ratio and a halving of the initial yield strength at 10 GPa and above, or else an absence of purely elastic behavior at these stresses during the time scale of shock experiments. The release wave profiles at 40 GPa suggest a similar yield behavior, but the Poisson's ratio of 0.347 calculated from the velocity of the inital release seems more acceptable as representing truly elastic behavior.

The $\epsilon \rightarrow \alpha$ reverse phase transition stress was determined for the first time in shock experiments as 9.8

±0.4 GPa. The accuracy of this measurement is much better than corresponding measurements under quasi-static conditions.[19,20] A useful application of the shock measurement of the reverse phase-transition stress may be in the calibration of in-material stress transducers such as the manganin gauge.[54] These devices are sometimes thought to exhibit a hysteresis in output on unloading, and thus a calibration point on the unloading path may be valuable.

ACKNOWLEDGMENTS

The authors gratefully acknowledge very helpful conversations with Dr. J.R. Asay, Dr. D.B. Hayes, R.A. Graham, Dr. J.W. Forbes, and Professor G.E. Duvall. Mrs. E.G. Young provided valuable computational assistance, and much encouragement and support were offered by Dr. D.E. Munson and Dr. W. Herrmann.

*Work supported by the United States Atomic Energy Commission.

†Present address: Terra Tek, Inc., 420 Wakara Way, Salt Lake City, Utah.

[1]D. Bancroft, E.L. Peterson, and S. Minshall, J. Appl. Phys. **27**, 291 (1956).
[2]J.C. Jamieson and A.W. Lawson, J. Appl. Phys. **33**, 776 (1962).
[3]T. Takahashi and W.A. Bassett, Science **145**, 483 (1964).
[4]R.L. Clendenen and H.G. Drickamer, J. Phys. Chem. Solids **25**, 865 (1964).
[5]J.M. Walsh, M.H. Rice, R.G. McQueen, and F.L. Yarger, Phys. Rev. **108**, 196 (1957).
[6]L.V. Al'tshuler, K.K. Krupnikov, B.N. Ledenev, V.I. Zhuchikhin, and M.I. Brazhnik. Sov. Phys.-JETP **7**, 606 (1958).
[7]R.G. McQueen and S.P. Marsh, J. Appl. Phys. **31**, 1253 (1960).
[8]D.S. Hughes, L.E. Gourley, and M.F. Gourley, J. Appl. Phys. **32**, 624 (1961).
[9]F.S. Minshall, in *Response of Metals to High Velocity Deformation*, edited by P.G. Shewmon and V.F. Zackay (Interscience, New York, 1961).
[10]L.V. Al'tshuler, A.A. Bakanova, and R.F. Trunin, Sov. Phys.-JETP **15**, 65 (1962).
[11]K.K. Krupnikov, A.A. Bakanova, M.I. Brazhnik, and R.F. Trunin, Sov. Phys.-JETP **8**, 205 (1963).
[12]J.W. Taylor and M.H. Rice, J. Appl. Phys. **34**, 364 (1963).
[13]T.R. Loree, C.M. Fowler, E.G. Zukas, and F.S. Minshall, J. Appl. Phys. **37**, 1918 (1966).
[14]S.A. Novikov, I.I. Divnov, and A.G. Ivanov, Sov. Phys.-JETP **20**, 545 (1965).
[15]Y. Horie and G.E. Duvall, in *Proceedings of the U.S. Army Symposium on Solid Mechanics, Watertown, Mass.*, 1968 (unpublished.)
[16]Y. Horie and G.E. Duvall, in *Behavior of Dense Media Under High Dynamic Pressure* (Gordon and Breach, New York, 1968).
[17]L.M. Barker and R.E. Hollenbach, J. Appl. Phys. **43**, 4669 (1972).
[18]D.R. Curran, in *Shock Waves and the Mechanical Properties of Solids*, edited by J.J. Burke and V. Weiss (Syracuse University Press, New York, 1971).
[19]P.M. Giles, M.H. Longenbach, and A.R. Marder, J. Appl. Phys. **42**, 4290 (1971).
[20]T. Takahashi, W.A. Bassett, and H.K. Mao, J. Geophys. Res. **73**, 4717 (1968).
[21]J.R. Asay and L.M. Barker, J. Appl. Phys. **45**, 2540 (1974).
[22]L.M. Barker and K.W. Schuler, J. Appl. Phys. **45**, 3692 (1974).
[23]L.M. Barker and R.E. Hollenbach, J. Appl. Phys. **41**, 4208 (1970).
[24]L.M. Barker, in *Behavior of Dense Media Under High Dynamic Pressures* (Gordon and Breach, New York, 1968).
[25]L.M. Barker and R.E. Hollenbach, Rev. Sci. Instrum. **36**, 1617 (1965).
[26]R.E. Hollenbach, Sandia Laboratories Report No. SLA-73-0830, 1973 (unpublished).
[27]L.M. Barker and R.E. Hollenbach, Rev. Sci. Instrum. **35**, 742 (1964).
[28]R.E. Hollenbach, Rev. Sci. Instrum. **43**, 1851 (1972).
[29]J.W. Forbes, Ph.D. thesis (Washington State University, 1974 (unpublished).
[30]Experiment 20 was a preliminary test using a 3-mm-thick specimen. Its profile appears as Fig. 5 in Ref. 17. Note, however, that the free-surface velocities in that figure must be corrected by dividing by 1.024, as explained in Ref. 22.
[31]O.E. Jones, F.W. Neilson, and W.B. Benedick, J. Appl. Phys. **33**, 3224 (1962).
[32]J.R. Holland, Acta Metall. **15**, 691 (1967).
[33]J.N. Johnson and R.W. Rhode, J. Appl. Phys. **42**, 4171 (1971).
[34]R.G. McQueen, S.P. Marsh, J.W. Taylor, J.N. Fritz, and W.J. Carter, in *High Velocity Impact Phenomena*, edited by Ray Kinslow (Academic, New York, 1970), p. 399.
[35]Intramaterial interfaces are produced when the material close to the free surface experiences a stress-volume history which is different from that at points far removed from the free surface. The difference in stress-volume history is caused by the reflections of the first-arriving waves from the free surface and their subsequent attenuation of the stresses behind later-arriving waves before the latter reach the free surface.
[36]The 0.5% late-time velocity increase was calculated by the SWAP-9 code (Ref. 39) using the equation of state which best fit the compressive and release wave profiles of experiment 15. The SWAP-9 code specifically states the magnitude of intramaterial interface reflections.
[37]O.E. Jones and R.A. Graham, In *Accurate Characterization of the High-Pressure Environment*, edited by E.C. Lloyd, Natl. Bur. Stand. Special Publication No. 326 (U.S. GPO, Washington, D.C., 1971).
[38]J.R. Asay (private communication).
[39]L.M. Barker and E.G. Young, Sandia Laboratories, Report No. SLA-74-0009, 1974 (unpublished).
[40]This value was obtained from $C_0^2 = (\lambda + 2/3\mu)\rho_0^{-1}$, where λ and μ are the Lamé constants and ρ_0 is the density, which is 7.85 g/cm^3. Values of the Lamé constants were taken from the *American Institute of Physics Handbook*, 3rd ed. (McGraw-Hill, New York, 1972), pp. 3—104.
[41]J.N. Johnson, D.B. Hayes, and J.R. Asay, J. Phys. Chem. Solids **35**, 501 (1974).
[42]L.M. Barker, C.D. Lundergan, and W. Herrmann, J. Appl. Phys. **35**, 1203 (1964).
[43]J.W. Taylor, in *Proceedings of Battelle Materials Science Colloquium*, edited by A.R. Rosenfield and G.T. Hahn (McGraw-Hill, New York, 1967), p. 573.
[44]The Hugoniot slope was found from Andrews' thermodynamically consistent equation of state for iron (Ref. 49).
[45]L.V. Al'tshuler, S.B. Kormer, M.I. Brazhnik, L.A. Vladimirov, M.P. Speranskaya, and A.I. Funtikov, Sov. Phys.-JETP **11**, 766 (1960).
[46]J.O. Erkman, J. Appl. Phys. **32**, 939 (1961).
[47]A.G. Ivanov and S.A. Novikov, Sov. Phys.-JETP **13**, 1321 (1961).
[48]The temperature of 350 K was estimated by D.B. Hayes (private communication) using the thermodynamically consistent equation of state for iron developed by Andrews (Ref. 49).
[49]D.J. Andrews, J. Phys. Chem. Solids **34**, 825 (1973).
[50]D.N. Pipkorn, C.K. Edge, P. Debrunner, G. De Pasquali, H.G. Drickamer, and H. Frauenfelder, Phys. Rev. **139**, A 1604 (1964).
[51]E.B. Royce, in *Behavior of Dense Media Under High Dynamic Pressures* (Gordon and Breach, New York, 1968).
[52]D.R. Curran and U. Hornemann (unpublished).
[53]By equilibrium value for the onset of the $\alpha \rightarrow \epsilon$ phase transition, we mean the stress to which the P1 wave would decay after a very long propagation distance, rather than the stress level at which the α and ϵ phases have equal Gibbs energies.
[54]D.D. Keough and J.Y. Wong, J. Appl. Phys. **41**, 3508 (1970).